To appear in ACM TOG 30(4).

A Quantized-Diffusion Model for Rendering Translucent Materials

Eugene d'Eon* Geoffrey Irving†
Weta Digital

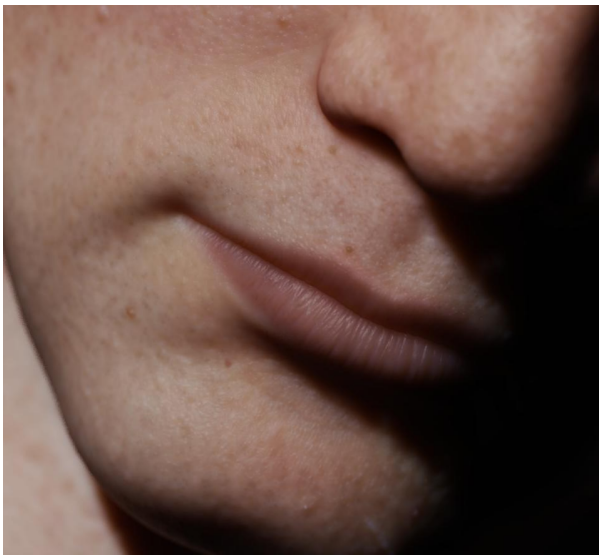

(a) Dipole (Jensen et al. 2001)

(b) Quantized-Diffusion

Figure 1: *Rendering a human face using a single-layer skin model. The classical dipole model (a) is frequency-limited and results in a waxy-looking appearance, particularly on the lips. A multipole model can create very realistic results, but requires additional material parameters which are difficult to measure and unintuitive to edit. Our quantized-diffusion model (b) produces accurate all-frequency subsurface scattering, achieves much of the realism of multilayer models and allows easy appearance editing.*

Abstract

We present a new BSSRDF for rendering images of translucent materials. Previous diffusion BSSRDFs are limited by the accuracy of classical diffusion theory. We introduce a modified diffusion theory that is more accurate for highly absorbing materials and near the point of illumination. The new diffusion solution accurately decouples single and multiple scattering. We then derive a novel, analytic, extended-source solution to the multilayer searchlight problem by quantizing the diffusion Green's function. This allows the application of the diffusion multipole model to material layers several orders of magnitude thinner than previously possible and creates accurate results under high-frequency illumination. Quantized diffusion provides both a new physical foundation and a variable-accuracy construction method for sum-of-Gaussians BSSRDFs, which have many useful properties for efficient rendering and appearance capture. Our BSSRDF maps directly to previous real-time rendering algorithms. For film production rendering, we propose several improvements to previous hierarchical point cloud algorithms by introducing a new radial-binning data structure and a doubly-adaptive traversal strategy.

CR Categories: I.3.7 [Computer Graphics]: Three-Dimensional Graphics and Realism—Radiosity;

Keywords: Subsurface scattering, BSSRDF, reflection models, layered materials, transport theory, diffusion, searchlight problem

*email:edeon@wetafx.co.nz
†email:irving@naml.us

Links: DL PDF WEB

1 Introduction

Rendering translucent materials is an important and challenging problem in computer graphics. All non-conducting surfaces (dielectrics) exhibit some level of subsurface scattering and absorption. The accurate and efficient simulation of these effects is often required to achieve the color and soft appearance of media such as skin, hair, ocean water, wax and marble. Local reflectance models are insufficiently accurate for this task when the scale of the image is such that significant levels of light survive subsurface transport at distances wider than a pixel. A *bidirectional scattering-surface reflectance-distribution function* (BSSRDF) is required to describe such non-local subsurface transport.

This paper presents a new analytic BSSRDF for scattering within multilayer translucent materials with arbitrary levels of absorption, very thin layers, and under all-frequency illumination. Our model

builds on previous analytic methods, making it efficient to evaluate and easy to integrate into existing software. We improve upon previous analytic models by not forcing all light to a single depth below the surface before scattering. Such single-depth models are inaccurate under high-frequency illumination (for example, near shadow boundaries) (see Figure 1). We derive an analytic model that considers all depths and avoids explicitly placing and contributing from internal sources in a 3D volume. The contribution from many depth sources at once arises from the separability of Gaussian functions and is applied to diffusion theory by temporally quantizing the diffusion Green's function.[1] Boundary conditions are solved using the method of images and the model is applied to material layers by use of a new extended multipole model. Together with the modifications to diffusion theory the extended multipole can describe multiple scattering within very thin layers.

We begin in the next section with a mathematical description of the problem and relation to previous work. In Section 3 we highlight several limitations of classical diffusion theory, motivating the need for a modified theory. Section 4 introduces a number of diffusion modifications from various other fields which are required for our new model and also improve previous diffusion models used in graphics. In Section 5 we derive a novel quantized-diffusion (QD) model, which makes the extended multipole model practical in graphics. We conclude our contributions in Section 7, presenting a number of methods for increasing the quality and efficiency of BSSRDF rendering algorithms based on irradiance caches.

2 Transport Theory

A description of subsurface light transport is typically made at an approximate level, avoiding the full complexity of Maxwell's equations. Linear transport theory [Case and Zweifel 1967] describes light or particle propagation through random media at the mesoscopic level and is the standard framework for simulating light transport in computer graphics [Kajiya and von Herzen 1984; Kajiya 1986]. In this framework, a scattering and absorbing medium is completely characterized by the index of refraction η together with the distribution and properties of absorbing and scattering particles. Given the *number densities* ρ_k of (possibly several) absorbers with *absorption cross-sections* σ_{ak} the resulting *absorption coefficient*[2] is $\mu_a = \sum_k \rho_k \sigma_{ak}$. The *scattering coefficient* $\mu_s = \sum_k \rho_k \sigma_{sk}$, together with the *phase function* $p(\vec{\omega}, \vec{\omega}')$, define the behaviour of individual scattering events. The phase function is a normalized distribution function for scattering deflections commonly parametrized by the *mean cosine of the deflection angle*, $g \in [-1, 1]$. We denote the *extinction coefficient* $\mu_t = \mu_a + \mu_s$ and the *single-scattering albedo* $\alpha = \mu_s / \mu_t$.

The key continuity equation for linear transport theory, which arises from a derivation of energy conservation [Williams 1971] or from more rigorous connections to Maxwell's equations [van Rossum and Nieuwenhuizen 1999; Mishchenko 2007], is the *linearized Boltzmann transport equation*

$$\vec{\omega} \cdot \nabla L(\vec{x}, \vec{\omega}) = -\mu_t L(\vec{x}, \vec{\omega}) + \mu_s \int_{4\pi} L(\vec{x}, \vec{\omega}') p(\vec{\omega}, \vec{\omega}') d\omega' + Q(\vec{x}, \vec{\omega}). \quad (1)$$

[1] All occurrences of the time variable in this paper refer to the evolution of photon distributions at time scales many orders of magnitude smaller than the shutter speed and are unrelated to animation.

[2] Following optics, we distinguish between the cross-sections σ of particles $[m^2]$ and coefficients μ of the medium $[m^{-1}]$. The difference has been previously blurred in other fields, occasionally leading to equations with inconsistent units.

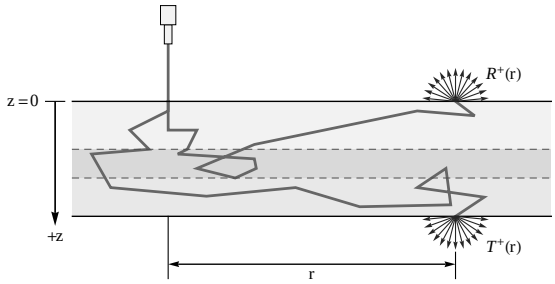

Figure 2: *The layered 2D searchlight problem is that of finding the energy reflected $R(r)$ and transmitted $T(r)$ through a layered scattering material as a function of distance r from the point of illumination by a focused beam.*

Its solution, subject to boundary conditions, provides the radiance $L(\vec{x}, \vec{\omega})$ at each position $\vec{x}$ and direction along unit vector $\vec{\omega}$ due to a given source distribution $Q(\vec{x}, \vec{\omega})$.

2.1 Related Work

Many exact solutions to the transport equation are known for symmetries where the radiance within the material $L(\vec{x}, \vec{\omega})$ varies only with a scalar spatial coordinate [Case and Zweifel 1967]. Several such 1D solutions[3] have been applied in graphics [Blinn 1982; Hanrahan and Krueger 1993; Stam 2001]. In order to support high-frequency illumination and produce truly non-local reflectance, higher dimensional geometries are required and exact solutions to these problems are rare. A largely successful compromise in graphics pioneered by Jensen et al. [2001] is the application of approximate solutions of a 2D version of the searchlight problem to general, curved surfaces. This approach greatly reduces the complexity of the problem and supports approximate angular incident and exitance variation by factoring the full BSSRDF into a product of Fresnel terms and a radially symmetric function.

2.1.1 The Searchlight Problem

Within the framework of transport theory, the exact BSSRDF for a flat, laterally-homogeneous material follows immediately from the solution to a problem posed in astrophysics known as the *searchlight problem* [Chandrasekhar 1958]: the problem of determining the exitant radiance at all positions and directions on a flat, laterally infinite surface due to illumination at a single point and in a single direction by a focused parallel beam (Figure 2). Rendering a full range of natural translucent materials requires a solution of the layered searchlight problem subject to arbitrary absorption levels, general phase functions, and supporting rough Fresnel interfaces. We mention an important collection of *exact* searchlight solutions, which, to the best of our knowledge, have not been previously recognized by the computer graphics community. Of particular interest are the recent 3D solutions given by Williams [2007; 2009]. These solutions are computationally expensive and restricted to isotropic semi-infinite media, which limits their use in rendering, but they provide a benchmark for validating both Monte Carlo reference implementations and approximate BSSRDFs. An extensive list of other exact searchlight solutions can be found in [Williams 2007].

Monte Carlo methods such as path tracing [Kajiya 1986] and photon mapping [Jensen et al. 1999] are very accurate, but exhibit extremely long convergence times for many common materials such

[3] These solutions describe the transport of light in a 3D medium with a symmetry such that the solution varies only with one scalar spatial coordinate, producing fundamentally 1D equations to solve.

as skin. Pharr and Hanrahan [2000] used the method of invariant imbedding to numerically evaluate very general BSSRDFs. This technique, while faster than standard Monte Carlo methods, is still computationally expensive.

Lacking an efficient exact solution to the layered searchlight problem, we turn to approximate methods. The diffusion approximation [Stam 1995] has led to several very practical solutions of a 2D searchlight problem using a dipole [Jensen et al. 2001] and later extended to multilayered materials with a multipole [Donner and Jensen 2005]. The one-depth source model used by these methods limits the frequency content of the reflected light and prevents the application of the multipole to thin material layers. An extended-source model was used by Donner and Jensen [2007], but must be numerically integrated and cannot accurately predict reflectance from thin materials because a reflectance multipole is not used.

Previously proposed diffusion methods in graphics have adopted classical diffusion theory, which has several known limitations [Davison 1957]. We introduce a modified diffusion theory that overcomes some of these limitations, improving both the accuracy of previous methods and our new BSSRDF. The telegrapher equation is an alternative modification to diffusion theory [Weinberg and Wigner 1958; Durian and Rudnick 1999], but has no closed form solution for extended sources and is not as accurate near the beam as our QD model. Other forms of modified diffusion theory [Grosjean 1963; Larsen 2010] include a rigorous diffusion length, but this is unlikely to have any measurable impact in graphics. Hybrid Monte-Carlo-diffusion techniques, such as [Li et al. 2005], can also benefit from modified diffusion theory.

Donner et al. [2009] presented an empirical 3D searchlight BSSRDF built on extensive Monte Carlo simulation that does not assume the radial symmetry of 2D searchlight solutions and can describe angular incident and exitant variation. However, their BSSRDF is limited to one-layer, infinitely thick materials with non-rough surfaces. Furthermore, their BSSRDF has not been compared to any exact transport solutions and is limited in resolution and range of parameters.

Our QD model produces Gaussian photon distributions around a point source. An explicit derivation for such distributions after n scattering events was given and applied for thermal neutron transport by Grosjean [1951]. This is less flexible than a temporal quantization and known to be inaccurate for low n. Similar distributions were noticed in Monte Carlo simulations by several authors [Spott and Svaasand 2000; Bouthors et al. 2008] who fit Gaussians to these empirically. Stam [1995] used Gaussian blobs to accelerate 3D finite element diffusion algorithms. Premoze et al. [2004] used Gaussian point spread functions placed along an extended source inside of heterogeneous scattering volumes. None of these works exploited the separability of Gaussians for computing accurate flux distributions at surfaces with Fresnel reflectance.

2.1.2 Other Approaches

We have mentioned primarily techniques that provide 2D or 3D layered searchlight solutions considering Fresnel reflection at the interface. We refer the reader to the survey by Cerezo et al. [2005] and to the references in [Pharr and Hanrahan 2000] for a wider background on solving the transport equation in graphics.

3 Classical Diffusion Theory

The difficulty of solving the transport equation is reduced by considering angular integrals of the radiance. The *P_N approximation* is obtained by expanding the transport equation in spherical harmonics, truncating the expansion at order N and imposing energy conservation [Weinberg and Wigner 1958]. For steady-state problems with $N = 1$ this process produces the *diffusion approximation*. Denoting the first two moments of the radiance as *fluence* ϕ (which is proportional to photon density) and *flux vector* $\vec{E}$:

$$\phi(\vec{x}) = \int_{4\pi} L(\vec{x},\vec{\omega})\, d\omega, \qquad \vec{E}(\vec{x}) = \int_{4\pi} L(\vec{x},\vec{\omega})\vec{\omega}\, d\omega,$$

the radiance everywhere within the medium is limited to

$$L(\vec{x},\vec{\omega}) \approx \frac{1}{4\pi}\phi(\vec{x}) + \frac{3}{4\pi}\vec{E}(\vec{x})\cdot\vec{\omega}. \tag{2}$$

The fluence satisfies the *diffusion equation*

$$-D\,\nabla^2\phi(\vec{x}) + \mu_a\phi(\vec{x}) = Q(\vec{x}) \tag{3}$$

where Q is an isotropic source function and D is the *diffusion coefficient* (defined below). In an infinite homogeneous medium with a unit power isotropic point source the solution of Equation (3) is the *diffusion Green's function*

$$\phi(r) = \frac{1}{4\pi D}\frac{\mathrm{e}^{-\sqrt{\frac{\mu_a}{D}}r}}{r}, \tag{4}$$

which forms the foundation of most practical analytic BSSRDFs. Our investigation of the accuracy of Equation (4) for high absorption, near sources and for building decoupled single- and multiple-scattering functions has led us to a modified diffusion theory that is well suited to image synthesis.

c	*speed of light in medium* [m/s]
η	*relative index of refraction*
ρ	*number density of particles* [m^{-3}]
σ_a	*absorption cross-section* [m^2]
σ_s	*scattering cross-section* [m^2]
$\mu_a = \sum_k \rho_k \sigma_{ak}$	*absorption coefficient* [m^{-1}]
$\mu_s = \sum_k \rho_k \sigma_{sk}$	*scattering coefficient* [m^{-1}]
$\mu_s' = (1-g)\mu_s$	*reduced scattering coefficient* [m^{-1}]
$\mu_t = \mu_s + \mu_a$	*extinction coefficient* [m^{-1}]
$\mu_t' = \mu_s' + \mu_a$	*transport coefficient* [m^{-1}]
$\alpha = \mu_s/\mu_t$	*single-scattering albedo*
$\alpha' = \mu_s'/\mu_t'$	*reduced single-scattering albedo*
$\ell = 1/\mu_t$	*mean free path (mfp)* [m]
$\ell' = 1/\mu_t'$	*reduced mean free path (mfp)* [m]
$p(\vec{\omega},\vec{\omega}')$	*phase function* [sr^{-1}]
g	*average cosine of scattering*
D	*diffusion coefficient* [m]
A	*reflection parameter*
$L(\vec{x},\vec{\omega})$	*radiance* [$\mathrm{W\,m^{-2}\,sr^{-1}}$]
$L_i(\vec{x},\vec{\omega})$	*incident radiance* [$\mathrm{W\,m^{-2}\,sr^{-1}}$]
$\vec{E}(\vec{x})$	*flux vector* [$\mathrm{W\,m^{-2}}$]
$\phi(\vec{x})$	*fluence* [$\mathrm{W\,m^{-2}}$]
$Q(\vec{x})$	*source function* [$\mathrm{W\,m^{-3}}$]

Table 1: *Nomenclature*

For much of the remainder of the paper we treat the important case of isotropic scattering ($g = 0$). A similarity relation is often used to reduce a problem with anisotropic scattering to an approximately equivalent isotropic problem with a *reduced scattering coefficient* $\mu_s' = (1-g)\mu_s$ and a related *transport coefficient* $\mu_t' = \mu_a + \mu_s'$. We discuss anisotropic scattering further in Section 10.

3.1 High Absorption and Near-Source Regimes

Several limitations of classical diffusion theory can be seen by considering a point source in an infinite homogeneous medium. The solution in Equation (4) to the diffusion equation (3) distributes

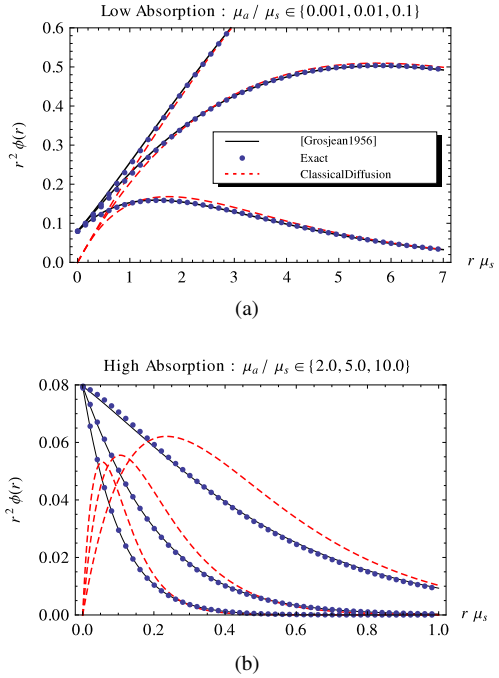

Figure 3: *Classical diffusion theory (dashed) poorly predicts photon density at small distances r from a point source in an infinite medium ($g = 0$). The errors increase for high absorption levels (b). Grosjean's approximation (7) (black) closely matches the exact transport solution, Equation (5) (dots).*

the correct number of photons, but at incorrect distances from the source. The error is greatest near the source where the true radiance is nearly mono-directional. This phenomenon cannot be represented by Equation (2) and the result is a severe underestimation of fluence very near the source and a somewhat lesser overestimation at distances comparable to the *mean free path* ($\ell = 1/\mu_t$). Figure 3 compares the classical diffusion result to the exact transport theory solution for isotropic scattering [Grosjean 1951; Case et al. 1953][4]:

$$\phi(r) = \frac{e^{-\mu_t r}}{4\pi r^2} + \frac{\mu_s}{2\pi^2 r}\int_0^\infty \frac{\arctan^2 u}{u - \alpha \arctan u}\,\sin(r\,\mu_t\,u)\,du. \qquad (5)$$

The classical diffusion solution is increasingly poor for high absorption levels (Figure 3b) because long scattering paths that arrive back at low r values are heavily absorbed, preventing the radiance from approaching a diffuse form. For all absorption levels the relative error decreases far from the source, but does not approach the correct asymptote [Case and Zweifel 1967].

3.2 Diffusion Coefficient and Closure

A common entry point for improving the accuracy of diffusion theory is to alter two of the somewhat arbitrary steps in its classical derivation. Substituting a P_N expansion of the radiance into the transport equation (1) yields a term of order $N+1$ and a closure must be chosen to yield a closed system of equations. The standard diffusion closure is Fick's law

$$\vec{E}(\vec{x}) = -D\,\nabla\phi(\vec{x}) \qquad (6)$$

which leads to Equation (3). Choosing an isotropic tensor-flux[5] yields the *classical diffusion coefficient* $D_{\mathrm{cl}} = 1/(3\mu_t')$. These are natural choices for closure and diffusion coefficient and have been rigorously derived from the transport equation through asymptotic analysis (along with boundary conditions that consider curvature [Malvagi and Pomraning 1991]), but nonetheless they have several limitations that have led to the development of entire families of modified diffusion theories and alternative diffusion coefficients [Minerbo 1978; Levermore and Pomraning 1981; Hauck and McClarren 2010].

[4] This integral is not absolutely convergent but can be transformed into a form suitable for numerical integration [Grosjean and Goovaerts 1985].

[5] An anisotropic tensor-flux can be used for anisotropic media [Jakob et al. 2010].

4 Modified Diffusion Theory

Methods for modifying diffusion theory have been studied for over sixty years, even in an asymptotically-consistent fashion [Larsen 2010]. However, the classical form of diffusion theory remains prevalent in the literature because no one modification is held to be universally superior for all problems. We found the following modifications useful for improving both previous diffusion models found in graphics and our new BSSRDF.

4.1 Grosjean's Approximation

A closed-form approximation from neutron transport [Grosjean 1956] for the fluence due to a point source in an infinite isotropically scattering medium is

$$\phi(r) = \frac{e^{-\mu_t' r}}{4\pi r^2} + \frac{1}{4\pi}\frac{3\mu_s'\mu_t'}{2\mu_a + \mu_s'}\frac{e^{-\sqrt{\frac{\mu_a}{D}}r}}{r} \qquad (7)$$

where

$$D = \frac{2\mu_a + \mu_s'}{3(\mu_a + \mu_s')^2}. \qquad (8)$$

Figure 3 compares Grosjean's approximation to exact transport and classical diffusion results. The approximation is accurate for all absorption levels and distances important for rendering. In our investigations we found it more accurate than other proposed approximations as found for instance in [Weinberg and Wigner 1958; Kim and Ishimaru 1998; Graaff and Rinzema 2001].

Equation (7) can immediately improve diffusion-based BSSRDFs by noting that the second term is the Green's function of a diffusion-type equation [Grosjean 1958]:

$$-D\,\nabla^2\phi(\vec{x}) + \mu_a\phi(\vec{x}) = \alpha' Q(\vec{x}) \qquad (9)$$

with a modified diffusion coefficient (8) and a source term weighted by the *reduced albedo* $\alpha' = \mu_s'/\mu_t'$. This suggests that adopting the modified diffusion coefficient in Equation (8) and multiplying the diffusion result by α' will provide a better description of the diffusive light than that predicted by classical diffusion. The energy not described by this modified diffusion solution, due to the first term in Equation (7), is the *ballistic fluence* leaving the point source unscattered. Later in the paper, as a beam of light enters a finite material and a subsurface source is placed at the point of first scatter, this ballistic fluence is precisely the single-scattered light leaving the material. Thus, when used in a BSSRDF, *Equation (7) provides an accurate decoupling of singly- and multiply-scattered light*. Much of the error in classical diffusion theory stems from not decoupling light in this way. The exact solution (5) and Grosjean's result (7) have a very similar shape and have identical zeroth moments, satisfying

$$\int_0^\infty 4\pi r^2\phi(r)dr = \frac{1}{\mu_a}. \qquad (10)$$

The classical diffusion result (4) attempts to encompass both ballistic and scattered fluence by satisfying Equation (10) with a single term that cannot describe the ballistic portion. Thus, adding single-scattering to classical diffusion BSSRDFs (or neglecting it entirely) leads to errors for absorbing materials (see Figure 4).

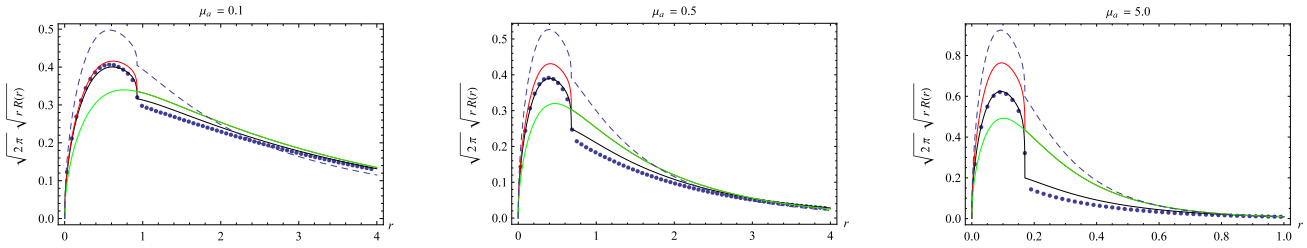

Figure 4: *Radiant emittance $R(r)$ for a semi-infinite medium with a unit point source at a depth of 1 mfp ($\eta = 1.4$, $\mu_s = 1, g = 0$). A diffusion dipole with the modifications from Section 4 closely matches Monte Carlo reference (circles) when added to a ballistic fluence term (black). The ballistic result is zero past the point where total internal reflection occurs. Using the classical diffusion Green's function with (red) or without (green) a ballistic term is less accurate. The errors in the infinite space solution (Figure 3) transfer directly to the semi-infinite case. The unmodified dipole solution from [Jensen et al. 2001] combined with a ballstic term exhibits additional error (dashed).*

4.2 Photon Diffusion Boundary Conditions

Applying diffusion theory to a medium with boundaries requires appropriate boundary conditions. The non-physical boundary conditions required by diffusion theory are typically derived in an *ad hoc* fashion. However, asymptotically-consistent boundary conditions for boundaries with Fresnel reflection have been derived [Pomraning and Ganapol 1995]. The variational approximation to the *linear-extrapolation distance* z_b given by this analysis is $z_b = 2AD$, with

$$A(\eta) = \frac{1 + 3\,C_2}{1 - 2\,C_1} \tag{11}$$

where C_i are hemispherical integrals of the *Fresnel reflectance* F_r,

$$C_i = \int_0^{\pi/2} F_r(\eta, \theta)\cos^i(\theta) sin(\theta) d\theta. \tag{12}$$

The *reflection parameter* A in Equation (11) improves upon previous solutions presented in graphics, which use only $F_{\mathrm{dr}} = 2C_1$ (see Figure 5). The result in Equation (11) was used for photon diffusion prior to its asymptotic derivation [Prahl 1988; Zhu et al. 1991]. We refer the reader to [Pomraning and Ganapol 1995] for the complete derivation, which considers a general BRDF applicable to rough surfaces. Analytic solutions for C_1 and C_2 are presented in [Aronson 1995]. We found the following approximations useful in our implementation

$$2\,C_1 \approx \begin{cases} 0.919317 - 3.4793\eta + 6.75335\eta^2 - 7.80989\eta^3 \\ \qquad +4.98554\eta^4 - 1.36881\eta^5, & \eta < 1 \\ -9.23372 + 22.2272\eta - 20.9292\eta^2 + 10.2291\eta^3 \\ \qquad -2.54396\eta^4 + 0.254913\eta^5, & \eta >= 1 \end{cases}$$

$$3\,C_2 \approx \begin{cases} 0.828421 - 2.62051\eta + 3.36231\eta^2 - 1.95284\eta^3 \\ \qquad +0.236494\eta^4 + 0.145787\eta^5, & \eta < 1 \\ -1641.1 + \frac{135.926}{\eta^3} - \frac{656.175}{\eta^2} + \frac{1376.53}{\eta} + 1213.67\eta \\ \quad -568.556\eta^2 + 164.798\eta^3 - 27.0181\eta^4 + 1.91826\eta^5, & \eta >= 1 \end{cases}$$

4.3 The Method of Images

An efficient method of solving diffusion boundary conditions is the *method of images* [Bryan 1890; Brinkworth 1964]. For the semi-infinite or finite-slab searchlight problems the *dipole* or *multipole* models approximately solve extrapolated boundary conditions by placing negative image sources outside the medium for every positive source inside and can be regarded as an approximate application of Placzek's Lemma [Case et al. 1953]. The radiance at the boundary is estimated by summing over all sources as if the medium extended throughout space. Perhaps unintuitively, the negative sources *increase* the net flux leaving the material.

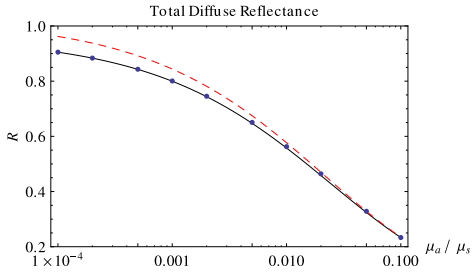

Figure 5: *The total diffuse reflectance (albedo) as a function of absorption μ_a/μ_s for an infinitely thick medium with $g = 0$, $\eta = 1.5$. The albedo is overestimated by more than 5% with the classical Fresnel reflection parameter (using only F_{dr}) (dashed). Using Eq. (11) (black) closely matches Monte Carlo (circles), producing more accurate colors when rendering with measured parameters.*

Solving a linear-extrapolation boundary condition exactly with the method of images requires a complex configuration of negative sources [Bryan 1890]. As pointed out by Durian and Rudnick [1999], placing a single negative source such that the fluence is zero at $-z_b$ is *not* an exact solution, especially for small r. However, this simplification is convenient and equivalent to the exact solution in the first two moments [Haskell et al. 1994]. We continue to adopt this simplification and note that more accurate solutions are given by Aronson [Aronson 1995] and Williams [Williams 2005].

4.3.1 The Searchlight Diffusion Source Function

Application of the method of images requires a point-source representation of the searchlight beam as it enters the media. The *extended-source function* [Grosjean 1958; Farrell et al. 1992] considers the location of all first-scatter events for the reduced-intensity beam as it passes through the medium. An isotropic point source is placed at every depth $z > 0$

$$Q(z) = \alpha' \mu_t' \, \mathrm{e}^{-\mu_t' z}. \tag{13}$$

Convolution of this extended-source function with the diffusion Green's function results in an integral with no closed form solution. A simpler model, which places all energy at a depth of exactly one mfp, is accurate for large distances from the beam but introduces considerable error near the beam and limits the application of the multipole model to materials thicker than several mfps (Figure 6). Additionally, all incident illumination, possibly with high-frequency variation due to surface detail or shadowing, is forced to a depth of 1 mfp and scatters isotropically from that depth. This light returns to the surface overly blurred and high frequency detail is lost (Figure 1). These limitations are the motivation for including an extended-source function in our BSSRDF.

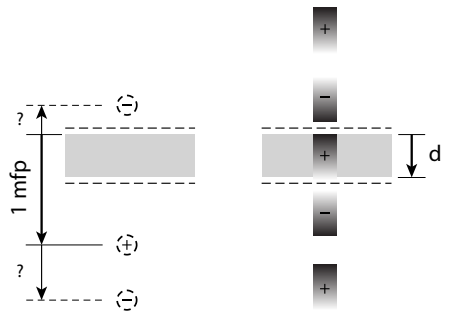

Figure 6: *The classical multipole (left) breaks down for thin layers because the first positive source lands below the layer. The extended multipole (right) mirrors continuous exponential sources about extrapolated boundaries.*

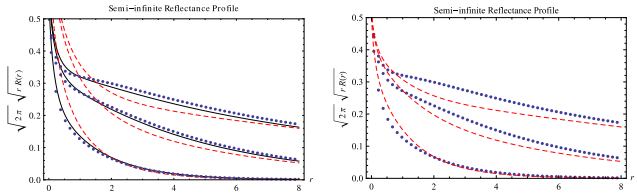

(a) (b)

Figure 7: *(a) An extended-source diffusion model (dashed-red) has considerable errors near the beam ($r = 0$) unless the KP exitance calculation in (14) is used (black). Monte Carlo reference is shown (dots) for comparison. Both diffusion solutions use Grosjean's diffusion equation (9) and add a single-scattering result. (b) Using the κ function from Donner and Jensen [2007] (dashed-red) improves the standard extended-source model, but the improved exitance calculation is consistently more accurate. Both plots show three absorption levels $\mu_a \in \{0.001, 0.05, 0.5\}$, with $\mu_s = 1, g = 0, \eta = 1.6$.*

4.3.2 Kienle-Patterson Exitance Calculation

Before deriving the new extended-source model we must revisit the calculation of exitant flux at a surface. Given the positive and negative source distributions for a given beam, previous methods [Jensen et al. 2001; Donner and Jensen 2005; Donner and Jensen 2007] use Fick's law (6):

$$R(r) = -D\nabla\phi(r, z = 0) \cdot (0, 0, -1)$$

where $\phi(r)$ is the sum of the fluence from all sources. However, the radiance at the boundary is better estimated by Equation (2) and a more accurate result considers the Fresnel transmittance $F_t(\eta, \theta)$ of this radiance for all exitant directions [Kienle and Patterson 1997]. The total exitance is then a linear combination of both the fluence and the flux at the surface:

$$R(r) = C_\phi\, \phi(r, z = 0) + C_{\vec{E}}(-D\nabla\phi(r, z = 0) \cdot (0, 0, -1)) \quad (14)$$

where $C_\phi = \frac{1}{4}(1 - 2C_1)$ and $C_{\vec{E}} = \frac{1}{2}(1 - 3C_2)$. Equation (14) significantly increases the accuracy of the method of images for sources near the boundary and is essential for our application of diffusion theory to thin materials. The extended source model is not consistently more accurate than the 1 mfp model when using Fick's law for computing exitance [Farrell et al. 1992]. However, with the Kienle-Patterson (KP) method the extended-source model is a considerable improvement (Figure 7a). Donner and Jensen [2007] improved the accuracy of near-surface sources with a κ function, but we found (14) consistently more accurate (Figure 7b).

5 A Practical Extended-Source Diffusion Model

Applying the extended source function (13) to a given Green's function $\Phi(r)$ requires evaluation of integrals of the form

$$\int_0^\infty \Phi(\sqrt{r^2 + z^2})\, Q(z)dz = \int_0^\infty \Phi(\sqrt{r^2 + z^2})\, \alpha' \mu_t' e^{-\mu_t' z} dz. \quad (15)$$

When Φ is the diffusion Green's function ϕ (or its gradient) Equation (15) has no closed form solution and must be numerically integrated for each distance of interest r from the point of illumination. However, if Φ is the 3D-normalized Gaussian of variance v

$$G_{3D}(v, r) = \frac{1}{(2\pi v)^{3/2}} e^{-r^2/(2v)}$$

then (15) produces a planar surface Gaussian of the same variance

$$\int_0^\infty G_{3D}(v, \sqrt{r^2 + z^2}) Q(z)dz = \frac{1}{2}\, \mu_s'\, f(\mu_t'^2 v/2)\, G_{2D}(v, r), \quad (16)$$

where $G_{2D}(v, r)$ is the 2D-normalized Gaussian

$$G_{2D}(v, r) = \frac{1}{2\pi v} e^{-r^2/(2v)},$$

and $f(x) = e^x \operatorname{erfc}(\sqrt{x})$ contains the complementary error function erfc. *A single evaluation of (16) provides an exact description of the fluence everywhere on the surface due to an extended Gaussian source*. This avoids many expensive numerical integrations. The application of this result requires a Gaussian Green's function or a finite Gaussian sum (exploiting linearity). The latter can be achieved by temporally quantizing the diffusion Green's function.

5.1 Quantized Diffusion

Particles or photons leaving a point source and undergoing diffusion produce Gaussian distributions with a mean displacement proportional to $\sqrt{tD}$ where t is the time since emission and D is the diffusion coefficient [Einstein 1905]. This is related to the steady-state Green's function (4) by integrating over contributions from all emission times t in the past [Patterson et al. 1989][6]

$$\frac{1}{4\pi D}\frac{e^{-r\sqrt{\frac{\mu_a}{D}}}}{r} = \int_0^\infty \frac{c}{(4\pi Dct)^{3/2}} e^{-\mu_a ct} e^{-r^2/(4Dct)} dt \quad (17)$$

where c is the speed of light in the medium. Equation (17) has a simple expression in terms of the normalized Gaussian

$$\frac{1}{4\pi D}\frac{e^{-r\sqrt{\frac{\mu_a}{D}}}}{r} = \int_0^\infty e^{-\tau\mu_a} G_{3D}(2D\tau, r)d\tau \quad (18)$$

where *time* $\tau = ct$ is measured in meters. *The distribution of photons at a time τ from emission grows as a 3D Gaussian of variance $v = 2D\tau$ centered at the source*. At time τ all photons have travelled a distance $\tau = ct$ so the entire Gaussian distribution is weighted by an absorption of $e^{-\tau\mu_a}$. Noting that these time-resolved distributions vary smoothly we build a discrete sum that closely approximates their continuous integral.

We quantize the time interval $\tau \in [0, \infty]$ by selecting $k + 1$ discrete time values τ_i with $\tau_0 = 0$ and $\tau_k = \infty$. We choose a weighted Gaussian $w_i\, G_{3D}(v_i, r)$ to approximate the distribution of photons

[6] In *classical* diffusion theory the integration for small time values is physically questionable for connecting the time-resolved and steady-state theories in this way [Pierrat et al. 2006]. We use the *modified* diffusion theory of Grosjean [1956] (for the scattered light only) which was fit to an exact transport solution. We require only the steady state result and (17) is used only to provide the Gaussian transform of our Green's function.

in flight within each time interval $[\tau_i, \tau_{i+1}]$. This produces a finite Gaussian expansion of the Green's function

$$\phi(r) = \int_0^\infty \mathrm{e}^{-\tau\mu_a} G_{3\mathrm{D}}(2D\tau, r)d\tau \approx \sum_{i=0}^{k-1} w_i\, G_{3\mathrm{D}}(v_i, r). \qquad (19)$$

The total absorption in the time interval $[\tau_i, \tau_{i+1}]$ provides an accurate choice for w_i

$$w_i = \int_{\tau_i}^{\tau_{i+1}} \mathrm{e}^{-\tau\mu_a} d\tau = \frac{\mathrm{e}^{-\tau_1\mu_a} - \mathrm{e}^{-\tau_2\mu_a}}{\mu_a}$$

and produces an expansion with a zeroth moment identical to that of the exact diffusion solution, ensuring the correct number of photons are distributed around the source with only slight error in their positioning. We found that choosing

$$\tau_i = s^{i-1}\tau_1 \qquad (20)$$

for $s \in [1.5, 2.0]$ produces an accurate and suitably sparse set of Gaussians. The variances v_i can be chosen using $v = 2D\tau$ by taking the average shape of the Gaussian in the time interval:

$$v_i = D(\tau_i + \tau_{i+1}).$$

Each successive Gaussian has a variance of s times the previous, which ensures a close representative Gaussian exists for any time τ. Absorption produces very small weights w_i for large time values, allowing a simple termination condition for selecting τ_{k-1}. Very small times also produce small weights and the scale of the problem being considered can be used to select τ_1 (see Section 7.1).

The following quantization with $s = (1+\sqrt{5})/2$

$$\phi(r) \approx \sum_{i=0}^{44} \frac{0.240606}{D}\, v_{\min}\, s^i\, \mathrm{e}^{-(v_{\min} s^i \mu_a/(2D))}\, G_{3\mathrm{D}}(v_{\min} s^i, r) \qquad (21)$$

is accurate to within 0.002% of the exact value for $r \in [5\sqrt{v_{\min}}, 60000\sqrt{v_{\min}}]$ over a wide range of albedos: for $\alpha = 0.9999$ (with $v_{\min} = 5 \times 10^{-5}/\mu_s^2$), for $\alpha = 0.5$ (with $v_{\min} = 5 \times 10^{-9}/\mu_s^2$), and for $\alpha = 0.1$ (with $v_{\min} = 10^{-10}/\mu_s^2$).

5.2 The Extended Multipole Model

A generalization of Equation (16) together with Equation (19) allows a new extended-multipole model for computing reflectance $R^{+/-}(r)$ and transmittance $T^{+/-}(r)$ profiles[7] for a finite material layer of thickness d. To compute exitance using the method of images and the KP exitance calculation (14), we require the total fluence and flux at depth $z = 0$, for R, and depth $z = d$, for T. The extended source function (13) creates an exponential distribution of primary sources inside the layer. Solving the boundary conditions using a multipole expansion mirrors these exponential distributions about the extrapolated boundaries (Figure 6). The extrapolation distances are based on the relative index of refraction at the top η_{top} and bottom η_{bottom} of the layer, $z_b(0) = 2A(\eta_{\text{top}})D$, $z_b(d) = 2A(\eta_{\text{bottom}})D$. An order-$n$ multipole expansion places an array of positive and negative sources offset from the primary sources by the following offsets [Donner and Jensen 2005]

$$m_{r,j} = 2j(d + z_b(0) + z_b(d))$$
$$m_{v,j} = 2j(d + z_b(0) + z_b(d)) - 2z_b(0)$$

where $j \in \{-n, n\}$ indexes each pair of positive (r) and negative (v) sources. Each source in this distribution produces fluence in the material using Grosjean's approximation (7). The ballistic term produces single-scattered light, which is accounted for separately. The remaining diffusion term employs a finite Gaussian expansion (19).

[7] We compute direction-dependent profiles $R^{+/-}(r)$ and $T^{+/-}(r)$ using the notation of [d'Eon et al. 2007]. The $(+)$ and $(-)$ profiles are not the same in general (and this is not a violation of reciprocity [Aronson 1997]).

Each Gaussian in this expansion produces planar Gaussian fluence and flux distributions at every depth z in the material. The generalization of Equation (16) for a finite layer with a Gaussian source offset a distance m from the primary source is a lateral 2D Gaussian with *fluence weight* w_ϕ,

$$\int_{z_1}^{z_2} Q(z) G_{3\mathrm{D}}(v, \sqrt{r^2 + (z+m)^2})dz = G_{2\mathrm{D}}(v, r) w_\phi(v, z_1, z_2, m),$$

$$w_\phi(v, z_1, z_2, m) = \int_{z_1}^{z_2} \frac{\mathrm{e}^{-\frac{(-z+m)^2}{2v}}}{\sqrt{2\pi v}} \alpha' \mu_t \mathrm{e}^{-\mu_t z} dz =$$

$$\frac{\alpha'\mu_t}{2} \mathrm{e}^{m\mu_t + \frac{\mu_t^2 v}{2}} \left(\mathrm{erf}\left[\frac{m + \mu_t v + z_2}{\sqrt{2v}}\right] - \mathrm{erf}\left[\frac{m + \mu_t v + z_1}{\sqrt{2v}}\right]\right).$$

The surface flux is also a Gaussian of variance v_i with weight $w_{\vec{E}}$ related to w_ϕ. Using Fick's law (6) and some manipulation yields

$$w_{\vec{E}}(v, z_1, z_2, m) = D\mu_t \Bigg[-w_\phi(v, z_1, z_2, m) + \frac{\alpha' \left(\mathrm{e}^{-\frac{m^2}{2v} - \frac{(m+\mu_t v)z_1}{v} - \frac{z_1^2}{2v}} - \mathrm{e}^{-\frac{m^2}{2v} - \frac{(m+\mu_t v)z_2}{v} - \frac{z_2^2}{2v}} \right)}{\sqrt{2\pi v}} \Bigg].$$

For each pair of sources j the *dipole reflectance fluence* and *flux weights*, $w_{\phi R}$ and $w_{\vec{E}R}$, are

$$w_{\phi R}(v, j) = w_\phi(v, 0, d, m_{r,j}) - w_\phi(v, 0, d, -m_{v,j})$$
$$w_{\vec{E}R}(v, j) = w_{\vec{E}}(v, 0, d, m_{r,j}) + w_{\vec{E}}(v, 0, d, -m_{v,j})$$

and the *total reflectance weight* $w_R(i)$ for Gaussian i is found by summing over all dipoles j in the multipole expansion and using the KP exitance calculation

$$w_R(i) = \sum_{j=-n}^{n} \left[C_\phi(\eta_{\text{top}}) w_{\phi R}(v_i, j) + C_{\vec{E}}(\eta_{\text{top}}) w_{\vec{E}R}(v_i, j) \right].$$

Summing contributions from all Gaussians i in the Green's function expansion and weighting the result by α' (see Section 4.1) produces the *downward reflectance profile*

$$R^+(r) = \alpha' \sum_{i=0}^{k-1} w_R(i)\, w_i G_{2\mathrm{D}}(v_i, r). \qquad (22)$$

The *downward transmittance profile* $T^+(r)$ is similar:

$$w_{\phi T}(v, j) = w_\phi(v, 0, d, -(d - m_{r,j})) - w_\phi(v, 0, d, d - m_{v,j})$$
$$w_{\vec{E}T}(v, j) = -w_{\vec{E}}(v, 0, d, -(d - m_{r,j})) - w_{\vec{E}}(v, 0, d, d - m_{v,j}),$$
$$w_T(i) = \sum_{j=-n}^{n} \left[C_\phi(\eta_{\text{bottom}}) w_{\phi T}(v_i, j) + C_{\vec{E}}(\eta_{\text{bottom}}) w_{\vec{E}T}(v_i, j) \right]$$
$$T^+(r) = \alpha' \sum_{i=0}^{k-1} w_T(i)\, w_i G_{2\mathrm{D}}(v_i, r)$$

The *upward profiles* $R^-(r)$ and $T^-(r)$ result from computing the respective downward profiles with η_{top} and η_{bottom} swapped. Semi-infinite materials use Equation (22) with $n = 0$ and $d = \infty$.

5.3 Multilayer Materials

Multiple scattering within layered materials can be computed by applying glass plates theory [Peraiah 2002] to lateral diffusion profiles, as shown by Donner and Jensen [2005; 2006]. Given QD profiles $R^{+/-}(r)$ and $T^{+/-}(r)$ for each layer, which are each sums of Gaussians, we compute reflectance and transmittance profiles for pairs of layers using a finite-order interlayer-scattering expansion similar to d'Eon et al. [2007]. We use a new convolution algorithm that does not require profiles with all integer powers of some narrowest variance (requiring 1000 Gaussians or more per profile).

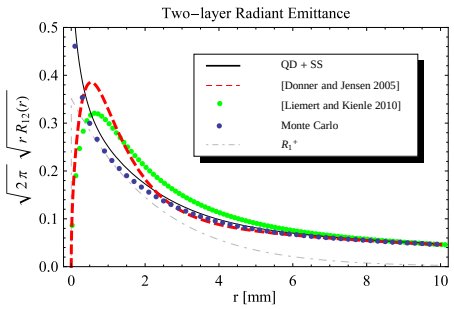

Figure 8: *Reflectance $R_{12}(r)$ from a 2-layer material. The top layer is 2 mfp thick with: $\mu_{a1} = 0.2\,mm^{-1}$, $\mu_{s1} = 1\,mm^{-1}$, $g_1 = 0$, $\eta_1 = 1.4$. The bottom layer is semi-infinite with $\mu_{a2} = 0.001\,mm^{-1}$, $\mu_{s2} = 0.5\,mm^{-1}$, $g_2 = 0$, $\eta_2 = 1.4$. The Quantized-Diffusion result added to single-scattering (black) closely matches Monte Carlo (dots). One-depth source models [Donner and Jensen 2005; Liemert and Kienle 2010] are frequency-limited due to errors near the beam. The diffuse reflectance for the top layer only R_1^+ is shown for comparison.*

The new algorithm (presented in Appendix A) takes as input two profiles relative to a common geometric sequence of Gaussians (constructed via Equation (21) with potentially 60 or more Gaussians) and provides an accurate result in terms of the same set of variances as the input profiles. This convolution operation is faster than previous methods and avoids the need for fast Fourier/Hankel routines and high radial resolutions (5000 radial samples are recommended by Donner and Jensen [2006]). In addition, there are no ringing artifacts and the albedo of the convolved profile is the product of the input profile albedos, providing exact energy conservation. For thin layers, a significant portion of the transmitted energy is unscattered, attenuated light passing directly through the layer. To incorporate this transmission in the otherwise diffusive interlayer scattering we add an additional Gaussian of zero variance to $T(r)$ profiles, $(1-(\frac{\eta_{top}-1}{\eta_{top}+1})^2)(1-(\frac{\eta_{bottom}-1}{\eta_{bottom}+1})^2)e^{-d\mu_t'}G_{2D}(0,r)$. A similar Gaussian added to $R(r)$ profiles, $(\frac{\eta_{top}-1}{\eta_{top}+1})^2 G_{2D}(0,r)$ roughly accounts for Fresnel reflection during interlayer-scattering.

6 Validation

We compared QD profiles to Monte Carlo simulations for reflectance and transmittance within homogeneous layers. We chose 16 absorption levels μ_a between 0.0001 and 10.0 and 9 layer thicknesses d from 0.02 mfp to 10.0 mfp with $g = 0$, $\eta_{\text{top}} = \eta_{\text{bottom}} = 1.4, \mu_s = 1$ and tested all combinations. A representative subset is shown in Figure 9 using a quantization with 40 Gaussians ($s = 1.618$). All Monte Carlo simulations used MCML [Wang et al. 1995]—an open source benchmark tool in medical physics. While not perfect matches, the QD solutions exhibit accurate behaviour at scales several orders of magnitude smaller than that for which they are typically applied. In the case of very thin materials, the scale of the plots are chosen to highlight the multiple scattering, with most of the energy directly transmitted through the material unscattered (appearing as a sharp peak near the beam). The QD results are globally more accurate than the classical multipole model.

Figure 8 shows a two-layer material profile computed with QD using the fast convolution algorithm with 60-Gaussian profiles and four interlayer scatterings. We compare to two recent methods for computing spatially-resolved multilayer profiles [Donner and Jensen 2005; Liemert and Kienle 2010], which both use 1-mfp source diffusion models and both result in frequency limited multilayer profiles due to errors near the beam.

7 Rendering with the QD BSSRDF

Exitant radiance at a surface location $\vec{x}_o$ in direction $\vec{\omega}_o$ is computed by convolving the incident radiance $L_i(x_i, \vec{\omega}_i)$ with a BSSRDF S:

$$L_o(x_o, \vec{\omega}_o) = \int_A \int_{2\pi} S(x_i, \vec{\omega}_i; x_o, \vec{\omega}_o) L_i(x_i, \vec{\omega}_i)(\vec{n} \cdot \vec{\omega}_i)\, d\omega_i\, dA(x_i).$$

Following Grosjean [1958], we separate light into reduced-intensity, single-scattering, and multiple-scattering components, each treated separately,

$$S = S^{(0)} + S^{(1)} + S_d.$$

Reduced-intensity transmission $S^{(0)}$ can be computed using standard transparency algorithms with depth dependent spectral absorption ($e^{-d\mu_t}$). Single scattering $S^{(1)}$ can be computed using previous methods such as the technique described in [Jensen et al. 2001]. Multiple scattering uses the QD model

$$S_d(x_i, \vec{\omega}_i; x_o, \vec{\omega}_o) = \frac{1}{\pi} F_t(x_i, \vec{\omega}_i) R(||x_i - x_o||_2) \frac{F_t(x_o, \vec{\omega}_o)}{4C_\phi(1/\eta)}, \quad (23)$$

where R is a sum of Gaussians computed with (22) for single-layered materials or from combinations of R and T profiles for multilayered materials (Appendix A). Equation (23) adds an additional normalization factor to the factorization of Jensen et al. [2001]: the diffusion profiles $R^{+/-}$ and $T^{+/-}$ provide the exitant scalar flux at material boundaries due to multiple scattering. The portion of light just below the surface that is reflected back into the medium is accounted for in solving the diffusion boundary conditions. The remaining flux leaving the surface is the value computed by Equation (22) and any heuristic used to estimate its angular shape should not remove or add energy. To use the angular shape $\frac{1}{\pi}F_t(x_o, \vec{\omega}_o)$ proposed by Jensen et al. [2001] we add the normalization factor $4C_\phi(1/\eta)$. More accurate exitant angular distributions can be computed as shown by Williams [2005]. Rough surfaces can be accounted for by replacing the Fresnel functions in Equations (12) and (23) with analogous integrals of the surface BRDF [Donner and Jensen 2005].

7.1 Choosing Quantizations

The general method described in Section 5.1 generates an infinite sequence of Gaussians. However, most of these have negligible weights when used to generate the surface diffusion profiles $R^{+/-}(r)$ and $T^{+/-}(r)$. With $s = 1.618$, 42 Gaussians are sufficient to account for 99.5% of the reflected energy for materials with a diffuse albedo less than 0.997. Fewer Gaussians can be used by increasing s, at the expense of some error in the profile shape. The weights w_i peak near $v \approx 2D/\mu_a$ and decreases monotonically for smaller and larger v. Depending on the scale of the object, material parameters, and resolution of the image, many Gaussians in the quantization will likely not move measurable energy into neighbouring pixels. All such narrow Gaussians can be approximated by a single one with a weight equal to the sum of all narrower Gaussian weights. As an object moves farther away in an image, more and more energy is represented by this narrowest Gaussian until the entire function is effectively local and evaluates like a bidirectional reflectance distribution function (BRDF).

7.2 Film Production Rendering

We implemented our QD BSSRDF for use in a visual effects pipeline using Photo-Realistic RenderMan (PRMan) extending the hierarchical irradiance point cloud algorithm of Jensen and Buhler [2002] in several ways. QD BSSRDF profiles are more expensive to evaluate, requiring up to 40 exponentials instead of the two of the dipole. However, the radial symmetry of the profiles can

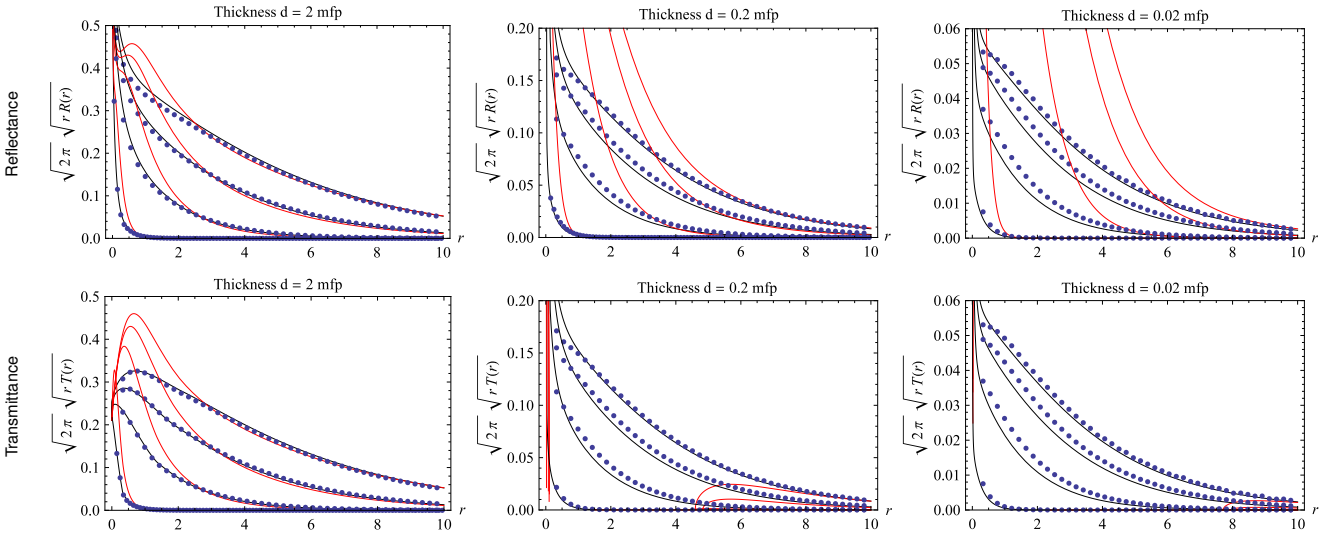

Figure 9: *Single layer Reflectance $R(r)$ and Transmittance $T(r)$ profiles for various thicknesses. Each plot shows four absorption levels $\mu_a \in \{0.0001, 0.1, 0.5, 5.0\}$ with $\mu_s = 1, g = 0, \eta_{top} = \eta_{bottom} = 1.4$. The red curves show the classical multipole [Donner and Jensen 2005] with single-scattering added. Even for optically thick layers (left) there is significant error near the beam due to the 1 mfp source model. Our QD extended-multipole model with single-scattering added (black) closely matches Monte Carlo simulation (dots) even for extremely thin slabs (right). The classical transmittance multipole goes highly negative for thin slabs do to the ill-behaved source placements (see Figure 6).*

be used to share many expensive calculations. The point cloud is stored in an octree and traversed for each render point as described in Jensen and Buhler [2002]. As each node in the octree is visited at render time, the irradiance is accumulated into a small 1D *radial binning* data structure instead of immediately evaluating the BSSRDF. After the energy from all octree nodes has been stored in the radial bins, the BSSRDF is analytically integrated over the width $[r_k, r_{k+1}]$ of each bin and multiplied by the total bin energy E_{bin}. *Many nodes in the point cloud, all at distances within $[r_k, r_{k+1}]$ from the render point, share a single BSSRDF evaluation $\int_{r_k}^{r_{k+1}} R(r)dr$.* The radial bin is then cleared for the next render point. We found 70 bins with a spacing of $r_k = r_1 + r_1 k 1.1^k$ sufficient for very smooth results. After all nodes have been accumulated the contribution from each bin k and for each Gaussian i in the BSSRDF is

$$\frac{E_{\text{bin}}[k]}{\pi(r_{k+1}^2 - r_k^2)} \left[\int_{r_k}^{r_k+1} 2\pi r G_{2\text{D}}(v_i, r)dr = \left(\mathrm{e}^{-r_k^2/(2v_i)} - \mathrm{e}^{-r_{k+1}^2/(2v_i)} \right) \right].$$

The analytic convolution of the profile over each bin shares exponential evaluations with neighbouring bins, providing a higher quality result while costing no more than the discrete evaluation proposed in [Jensen and Buhler 2002]. The use of analytic convolution reduces undersampling artifacts typical of narrow profiles, already reported in literature and for which a number of partial solutions have been proposed (see for example [Langlands and Mertens 2007] or [Neulander 2009]). The areas of each bin and all the exponentials can be computed once and reused for many calculations even if the profile changes, provided the set of variances remains the same, which can be enforced in the quantization of the profile.

For heterogeneous materials we store a weighted average of the values μ_a and μ_s' in the same radial binning structure. Each bin contribution averages material properties from radius 0 to radius r_{k+1} and updates the profile before integrating. All energy arriving from radius r_k considers the material properties between it and the render point instead of just properties at either 0 or r_k. Profile updates are quickly performed for arbitrary changes in μ_s' by a linear scaling of the variances. Small relative changes ($< 1\%$) in μ_a allow fast approximate updates by a simple rescaling of the Gaussian weights to sum to the new diffuse color R_d.

The octree method is further accelerated by noting that far away nodes contribute nearly identical results to nearby render points. As our implementation runs inside PRMan, it is already provided with batches of nearby points to be shaded at once, known as *micropolygon grids*. It is then quite natural to store these points into a small, local acceleration structure and use it to share contributions from far away nodes. This is similar to doubly-adaptive traversal strategies used in particle simulation [Greengard and Rokhlin 1997].

8 Discussion

Our QD BSSRDF generates sum-of-Gaussians scattering profiles which have several advantages over other BSSRDF representations:

- Convolving irradiance with a sum-of-Gaussians BSSRDF can be performed hierarchically and separably as in [d'Eon et al. 2007; Donner et al. 2008], where the profiles were generated using nonlinear optimization and empirical fitting. Our QD BSSRDF provides physical justification for these profiles and generates more accurate profiles orders of magnitude faster.
- Scattering properties of real materials have been measured using laser beam [Jensen et al. 2001] and structured light [Tariq et al. 2006] illuminations. A sum-of-Gaussians BSSRDF has a trivial convolution with Gaussian-beam and half-plane source functions making them ideal sources for estimating material parameters with our model. The basis is also well suited for capturing RGB profiles directly, which are the combination of many different pure-frequency profiles and often not well represented by any single set of scattering parameters (for example, skin). Precomputation and tabulation of profiles is efficient and compact.
- A wealth of exact transport and diffusion solutions are known only in Fourier space including all of the exact searchlight solutions from [Elliott 1955] to [Williams 2009]. A sum-of-Gaussians representation transforms trivially to and from Fourier space with no Gibbs phenomenon or precision issues and linearity of the Fourier transform permits fitting Gaussians to exact solutions in Fourier space, avoiding the limitations of traditional Fourier inversion.

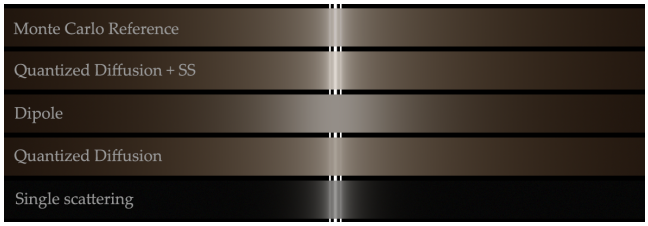

Figure 10: *Illumination of semi-infinite material with normally-incident, collimated, high-frequency white light. Different simulations are shown side by side with the vertical stripe illumination shown in between each image for comparison. The multiple scattering predicted by our QD model contains high-frequency details that the classical dipole model lacks. When added to single-scattering, the QD model closely matches the appearance of the Monte Carlo reference simulation. The QD model has more accurate, saturated colors than the dipole due to Grosjean's improved diffusion equation.*

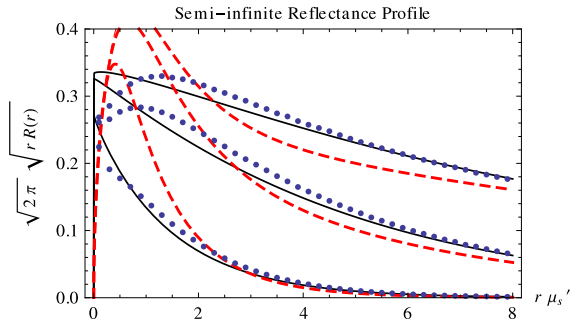

Figure 11: **Anisotropic Scattering***: Our QD model (black) is less precise for media with anisotropic scattering, but much closer to Monte Carlo simulation (dots) than the classical diffusion dipole (dashed-red). Three absorption levels are shown* $\mu_a/\mu_s' \in \{0.001, 0.05, 0.5\}$*, with* $g = 0.95, \eta = 1.6$.

9 Results

Figure 1 shows a comparison of single-layer BSSRDFs applied to skin. While skin is a multilayer material, measured multilayer parameters and difficult to acquire and unintuitive to edit. We found that it is possible to achieve very realistic results with our QD BSSRDF even for single-layer skin with parameters derived from painted maps of the albedo and scattering coefficient. The accurate profile shape for small radii keeps subtle detail that is lost by the dipole model. Figure 10 further illustrates the differences in frequency content and colours predicted by our model vs. the classical dipole model, showing reflectance from a homogeneous material with $g = 0$, $\mu_a = \{0.02, 0.05, 0.1\}$, $\mu_s = 1$, $\eta = 1.5$. Figure 12 (bottom-left) shows a PRMan render of a liquid animation using measured scattering properties of cream [Jensen et al. 2001] applied. The render time on a 6-CPU Xeon 2.66 GHz machine was 31 minutes per frame with 625 million profile evaluations from 9 million irradiance points with 45-Gaussian QD profiles. Comparison time for an optimized implementation of [Jensen and Buhler 2002] of the same scene was 15 minutes per frame. Figure 12 (bottom-right) shows further liquid animation results using milk parameters under area light illumination. Figure 12 (top) shows an application of the QD model to a textured alien. A deep translucence is achieved with a single-layer material model, keeping fine details that are lost with the dipole model at the same translucency. The radially-averaged texturing produces a complex heterogeneous appearance.

10 Limitations and Future Work

Grosjean's Green's function (7) fits an exact solution for isotropic scattering and is not exact for anisotropic scattering. While not as accurate as the profiles for isotropic scattering, anisotropic QD profiles using (7) are more accurate than previous analytic BSSRDFs (Figure 11). More accurate Green's functions for anisotropic scattering often include multiple occurrences of the basic diffusion Green's function (4), such as Grosjean's extension of his 1956 result to linear-anisotropic scattering [Grosjean 1957], infinite plane-wave expansions [Liemert and Kienle 2011], and simplified P_N methods [Larsen 2010]. Our quantized-diffusion methods can apply to these Green's functions via Equation (19). Possible extensions to angular sources include the methods of Williams [1978] and $\delta - P_N$ theory [Carp et al. 2004]. The Fokker-Planck approximation for highly forward scattering media also includes Gaussians [Pomraning 2000] and might offer extension of the ideas of QD to such materials.

The computation of multilayer profiles is limited by the methods in [Donner and Jensen 2005]—the multiply-scattered transmitted flux hitting the next layer does not arrive like a collimated beam, but as a diffuse surface source. Improving upon this requires a multi-flux version of [Donner and Jensen 2005], including an expansion of single-scattering within slabs in terms of Gaussians and a model for diffuse surface sources.

Our diffusion quantization provides a separation of the flux leaving the surface into Gaussian photon packets that have travelled different distances through the material. An area for future work is the use of this separation for building multiscale scattering functions where each Gaussian photon packet considers a different local average of material properties, surface normal and curvature for solving multiscale boundary conditions. This may further extend the accuracy of diffusion solutions within heterogeneous, curved media. Similarly, a sum of elliptically warped Gaussians could easily represent the stretched profiles seen in anisotropic media [Jakob et al. 2010] and describe the contrary stretching directions observed in the near and far field regimes [Kienle 2007]. These stretched Gaussians are seen in the time-resolved Green's function for anisotropic media [Dudko and Weiss 2005], which could also be quantized.

11 Conclusion

We have presented a new reflectance model for layered translucent materials. Our model builds on previous diffusion BSSRDFs with both a modified diffusion framework and a novel evaluation of the extended source function in a material layer. We have demonstrated significant impact of these changes in the colors of materials rendered with measured parameters, in the bleeding of light near high frequency features such as shadow edges, in the division of reflected light into single and multiple scattered components, and in the application of diffusion theory to very thin materials. Our model produces surface scattering functions in terms of Gaussian sums that have many advantages over alternate representations. We validated our model by comparing to exact transport solutions and benchmark Monte Carlo simulations. Our model is practical and currently in use at a major visual effects studio.

Acknowledgements

We would like to thank the SIGGRAPH reviewers. The authors are also indebted to Guillaume Francois, Luca Fascione, David Abbott, Jedrzej Wojtowicz, Joe Letteri, Sebastian Sylwan, Martin Hill, Michael Nielsen and Matt Hicks for help creating images for the

Figure 12: *Applications of our quantized-diffusion BSSRDF in production using PRMan.*

paper and help improving the exposition. Huge thanks to Andrei Coval, Keven Norris, and Gino Acevedo for the blacksmith face and to Bradford deCaussin for the octoguy model.

References

ARONSON, R. 1995. Boundary conditions for diffusion of light. *J. Opt. Soc. Am. A 12*, 11 (Nov), 2532–2539.

ARONSON, R. 1997. Radiative transfer implies a modified reciprocity relation. *J. Opt. Soc. Am. A 14*, 2 (Feb), 486–490.

BLINN, J. F. 1982. Light reflection functions for simulation of clouds and dusty surfaces. In *Computer Graphics (Proceedings of SIGGRAPH 82)*, ACM, vol. 16, 21–29.

BOUTHORS, A., NEYRET, F., MAX, N., BRUNETON, E., AND CRASSIN, C. 2008. Interactive multiple anisotropic scattering in clouds. In *Proceedings of the 2008 symposium on Interactive 3D graphics and games*, ACM, 173–182.

BRINKWORTH, B. J. 1964. A diffusion model of the transport of radiation from a point source in the lower atmosphere. *British Journal of Applied Physics 15*, 6, 733.

BRYAN, G. H. 1890. An application of the method of images to the conduction of heat. *Proceedings of the London Mathematical Society s1-22*, 1, 424–430.

CARP, S. A., PRAHL, S. A., AND VENUGOPALAN, V. 2004. Radiative transport in the delta-P_1 approximation: accuracy of fluence rate and optical penetration depth predictions in turbid semi-infinite media. *Journal of Biomedical Optics 9*, 3, 632–647.

CASE, K. M., AND ZWEIFEL, P. F. 1967. *Linear Transport Theory*. Addison-Wesley.

CASE, K. M., DE HOFFMAN, F., AND PLACZEK, G. 1953. *Introduction to the Theory of Neutron Diffusion*, vol. 1. US Government Printing Office.

CEREZO, E., PEREZ, F., PUEYO, X., SERON, F., AND SILLION, F. 2005. A survey on participating media rendering techniques. *The Visual Computer 21*, 5, 303–328.

CHANDRASEKHAR, S. 1958. On the diffuse reflection of a pencil of radiation by a plane-parallel atmosphere. *Proceedings of the National Academy of Sciences of the United States of America 44*, 9, 933–940.

DAVISON, B. 1957. *Neutron Transport Theory*. Oxford University Press.

D'EON, E., LUEBKE, D., AND ENDERTON, E. 2007. Efficient rendering of human skin. In *Rendering Techniques*, 147–157.

DONNER, C., AND JENSEN, H. W. 2005. Light diffusion in multilayered translucent materials. *ACM Trans. Graph. 24* (July), 1032–1039.

DONNER, C., AND JENSEN, H. W. 2006. Rapid simulation of steady-state spatially resolved reflectance and transmittance profiles of multilayered turbid materials. *J. Opt. Soc. Am. A 23*, 6 (Jun), 1382–1390.

DONNER, C., AND JENSEN, H. W. 2007. Rendering translucent materials using photon diffusion. In *Rendering Techniques*, 243–251.

DONNER, C., WEYRICH, T., D'EON, E., RAMAMOORTHI, R., AND RUSINKIEWICZ, S. 2008. A layered, heterogeneous reflectance model for acquiring and rendering human skin. *ACM Trans. Graph. 27*, 5 (Dec), 140:1–140:12.

DONNER, C., LAWRENCE, J., RAMAMOORTHI, R., HACHISUKA, T., JENSEN, H. W., AND NAYAR, S. 2009. An empirical BSSRDF model. *ACM Trans. Graph. 28* (July), 30:1–30:10.

DUDKO, O., AND WEISS, G. 2005. Estimation of anisotropic optical parameters of tissue in a slab geometry. *Biophysical journal 88*, 5, 3205–3211.

DURIAN, D. J., AND RUDNICK, J. 1999. Spatially resolved backscattering: implementation of extrapolation boundary condition and exponential source. *J. Opt. Soc. Am. A 16*, 4 (Apr), 837–844.

EINSTEIN, A. 1905. Über die von der molekularkinetischen Theorie der Wärme geforderte Bewegung von in ruhenden Flüssigkeiten suspendierten Teilchen. *Annalen der Physik 17*, 549–560.

ELLIOTT, J. P. 1955. Milne's problem with a point-source. *Proceedings of the Royal Society of London. Series A, Mathematical and Physical Sciences 228*, 1174, 424–433.

FARRELL, T. J., PATTERSON, M. S., AND WILSON, B. 1992. A diffusion theory model of spatially resolved, steady-state diffuse reflections for the noninvasive determination of tissue optical properties *in vivo*. *Med. Phys. 19*, 4, 879–888.

GRAAFF, R., AND RINZEMA, K. 2001. Practical improvements on photon diffusion theory: application to isotropic scattering. *Physics in Medicine and Biology 46*, 11, 3043.

GREENGARD, L., AND ROKHLIN, V. 1997. A fast algorithm for particle simulations. *Journal of Computational Physics 135*, 2, 280–292.

GROSJEAN, C. C., AND GOOVAERTS, M. J. 1985. On the series expansion of certain types of integral transforms–Part I. *Journal of Computational and Applied Mathematics 12*, 277–298.

GROSJEAN, C. C. 1951. The Exact Mathematical Theory of Multiple Scattering of Particles in an Infinite Medium. *Memoirs Kon. Vl. Ac. Wetensch. 13*, 36.

GROSJEAN, C. C. 1956. A high accuracy approximation for solving multiple scattering problems in infinite homogeneous media. *Nuovo Cimento 3*, 6 (Jun), 1262–1275.

GROSJEAN, C. C. 1957. Further development of a new approximate one-velocity theory of multiple scattering. *Il Nuovo Cimento 5*, 1, 83–101.

GROSJEAN, C. C. 1958. Multiple Isotropic Scattering in Convex Homogeneous Media Bounded by Vacuum. *Proceedings of the Second International Conference on the Peaceful Uses of Atomic Energy 16*, 413.

GROSJEAN, C. C. 1963. A new approximate one-velocity theory for treating both isotropic and anisotropic multiple scattering problems. Part I. Infinite homogeneous scattering media. Tech. rep., Universiteit, Ghent.

HANRAHAN, P., AND KRUEGER, W. 1993. Reflection from layered surfaces due to subsurface scattering. In *Proceedings of ACM SIGGRAPH 1993*, 165–174.

HASKELL, R. C., SVAASAND, L. O., TSAY, T.-T., FENG, T.-C., MCADAMS, M. S., AND TROMBERG, B. J. 1994. Boundary conditions for the diffusion equation in radiative transfer. *J. Opt. Soc. Am. A 11*, 10, 2727–2741.

HAUCK, C., AND MCCLARREN, R. 2010. Positive P_N closures. *SIAM Journal on Scientific Computing 32*, 5, 2603–2626.

JAKOB, W., ARBREE, A., MOON, J. T., BALA, K., AND MARSCHNER, S. 2010. A radiative transfer framework for rendering materials with anisotropic structure. *ACM Trans. Graph. 29* (July), 53:1–53:13.

JENSEN, H. W., AND BUHLER, J. 2002. A rapid hierarchical rendering technique for translucent materials. *ACM Trans. Graphic. 21*, 576–581.

JENSEN, H. W., LEGAKIS, J., AND DORSEY, J. 1999. Rendering of wet materials. In *Rendering Techniques*, 273–282.

JENSEN, H. W., MARSCHNER, S. R., LEVOY, M., AND HANRAHAN, P. 2001. A practical model for subsurface light transport. In *Proceedings of ACM SIGGRAPH 2001*, 511–518.

KAJIYA, J., AND VON HERZEN, B. 1984. Ray tracing volume densities. In *Computer Graphics (Proceedings of SIGGRAPH 84)*, ACM, 174.

KAJIYA, J. T. 1986. The rendering equation. In *Computer Graphics (Proceedings of SIGGRAPH 86)*, 143–150.

KIENLE, A., AND PATTERSON, M. S. 1997. Improved solutions of the steady-state and the time-resolved diffusion equations for reflectance from a semi-infinite turbid medium. *J. Opt. Soc. Am. A 14*, 1, 246–254.

KIENLE, A. 2007. Anisotropic light diffusion: An oxymoron? *Phys. Rev. Lett. 98*, 21 (May), 218104.

KIM, A. D., AND ISHIMARU, A. 1998. Optical diffusion of continuous-wave, pulsed, and density waves in scattering media and comparisons with radiative transfer. *Appl. Opt. 37*, 22 (Aug), 5313–5319.

LANGLANDS, A., AND MERTENS, T. 2007. Noise-free bssrdf rendering on the cheap. In *ACM SIGGRAPH 2007 posters*, ACM, 182.

LARSEN, E. 2010. Asymptotic diffusion and simplified P_N approximations for diffusive and deep penetration problems. part 1: Theory. *Transport Theory and Statistical Physics 39*, 2, 110–163.

LEVERMORE, C., AND POMRANING, G. 1981. A flux-limited diffusion theory. *The Astrophysical Journal 248*, 321–334.

LI, H., PELLACINI, F., AND TORRANCE, K. 2005. A hybrid monte carlo method for accurate and efficient subsurface scattering. In *Rendering Techniques*, 283–290.

LIEMERT, A., AND KIENLE, A. 2010. Light diffusion in N-layered turbid media: steady-state domain. *Journal of Biomedical Optics 15*, 2, 025003.

LIEMERT, A., AND KIENLE, A. 2011. Analytical solution of the radiative transfer equation for infinite-space fluence. *Physical Review A 83*, 1, 015804.

MALVAGI, F., AND POMRANING, G. C. 1991. Initial and boundary conditions for diffusive linear transport problems. *Journal of Mathematical Physics 32*, 3, 805.

MINERBO, G. 1978. Maximum entropy Eddington factors. *J. Quant. Spectrosc. Radiat. Transfer 20*, 6, 541–545.

MISHCHENKO, M. I. 2007. Radiative transfer: a new look of the old theory. In *Radiative Transfer–V*, Begell House, 1–30.

NEULANDER, I. 2009. Smoother subsurface scattering. In *SIGGRAPH 2009: Talks*, ACM, 1.

PATTERSON, M. S., CHANCE, B., AND WILSON, B. C. 1989. Time resolved reflectance and transmittance for the non-invasive measurement of tissue optical properties. *Appl. Opt. 28*, 12, 2331–2336.

PERAIAH, A. 2002. *An introduction to Radiative Transfer: Methods and Applications in Astrophysics*. Cambridge University Press.

PHARR, M., AND HANRAHAN, P. 2000. Monte carlo evaluation of non-linear scattering equations for subsurface reflection. In *Proceedings of ACM SIGGRAPH 2000*, 75–84.

PIERRAT, R., GREFFET, J.-J., AND CARMINATI, R. 2006. Photon diffusion coefficient in scattering and absorbing media. *J. Opt. Soc. Am. A 23*, 5 (May), 1106–1110.

POMRANING, G. C., AND GANAPOL, B. D. 1995. Asymptotically consistent reflection boundary conditions for diffusion theory. *Annals of Nuclear Energy 22*, 12, 787 – 817.

POMRANING, G. C. 2000. The transport theory of beams. *Transport Theory and Statistical Physics 29*, 1, 1–41.

PRAHL, S. 1988. *Light Transport in Tissue*. PhD thesis, University of Texas at Austin.

PREMOŽE, S., ASHIKHMIN, M., RAMAMOORTHI, R., AND NAYAR, S. 2004. Practical rendering of multiple scattering effects in participating media. In *Rendering Techniques*, 363–374.

SPOTT, T., AND SVAASAND, L. O. 2000. Collimated light sources in the diffusion approximation. *Appl. Opt. 39*, 34, 6453–6465.

STAM, J. 1995. Multiple scattering as a diffusion process. In *Rendering Techniques*, 41–50.

STAM, J. 2001. An illumination model for a skin layer bounded by rough surfaces. In *Rendering Techniques*, 39–52.

TARIQ, S., GARDNER, A., LLAMAS, I., JONES, A., DEBEVEC, P., AND TURK, G. 2006. Efficient estimation of spatially varying subsurface scattering parameters. In *Vision, Modeling, and Visualization*.

VAN ROSSUM, M., AND NIEUWENHUIZEN, T. 1999. Multiple scattering of classical waves: microscopy, mesoscopy, and diffusion. *Reviews of Modern Physics 71*, 1, 313–371.

WANG, L. V., JACQUES, S. L., AND ZHENG, L. 1995. MCML – monte carlo modeling of light transport in multi-layered tissues. *Computer Methods in Programs and Biomedicine 47*, 8, 131–146.

WEINBERG, A. M., AND WIGNER, E. P. 1958. *The Physical Theory of Neutron Chain Reactors*. University of Chicago Press.

WILLIAMS, M. M. R. 1971. *Mathematical methods in particle transport theory*. Butterworth.

WILLIAMS, M. M. R. 1978. A synthetic scattering kernel for particle transport in absorbing media with anisotropic scattering. *Journal of Physics D: Applied Physics 11*, 2455.

WILLIAMS, M. M. R. 2005. The Milne problem with Fresnel reflection. *Journal of Physics A: Mathematical and General 38*, 17, 3841.

WILLIAMS, M. M. R. 2007. The searchlight problem in radiative transfer with internal reflection. *Journal of Physics A: Mathematical and Theoretical 40*, 24, 6407.

WILLIAMS, M. M. R. 2009. Three-dimensional transport theory: An analytical solution of an internal beam searchlight problem, III. *Annals of Nuclear Energy 36*, 8, 1256 – 1261.

ZHU, J., PINE, D., AND WEITZ, D. 1991. Internal reflection of diffusive light in random media. *Physical Review A 44*, 6, 3948–3959.

A Fast sum-of-Gaussians Radial Convolution

Pseudo-code for an O(N) 2D radial convolution algorithm for two sum-of-Gaussians radially-symmetric functions. To approximate the convolution of two Gaussians $a_i G_{2D}(v_i, r)$ and $b_j G_{2D}(v_j, r)$, we find k s.t. $v_k \le v_i + v_j \le v_{k+1}$ and distribute weight $a_i b_j$ between the v_k and v_{k+1} Gaussians via

$$w_{k+1} = a_i b_j \frac{v_i + v_j - v_k}{v_{k+1} - v_k} \qquad w_k = a_i b_j - w_{k+1}$$

If $v_i = s^i v_0$ and $s \ge (1+\sqrt{5})/2 \approx 1.618$ all pairs (a_i, b_j) with $j < i$ fall between v_i and v_{i+1}, and can be computed all at once via

$$w_{i+1} = \frac{a_i}{v_{i+1} - v_i} \sum_{j<i} b_j v_j \qquad w_i = a_i \sum_{j<i} b_j - w_{i+1}$$

Precomputing the sums for all i yields an $O(n)$ algorithm:

```
// Assumes a[i] and b[i] are the weights for 2D normalized Gaussians with variances v[i]
// It is further assumed that v[i+1] = s * v[i], where s is the golden ratio
c[] fastconvolve( a[], b[], v[] )
{
  s = ( 1 + sqrt(5) ) / 2;
  oneoverr = 1 / s
  oneoverrm1 = oneoverr / ( s - 1 )
  N = length( v )
  c = zeros( N )
  suma = sumav = sumb = sumbv = 0
  // contribute from all off-diagonal pairs
  for( k = 0; k < N - 1; k++ )
    chi    = a[k] * sumbv + b[k] * sumav
    c[k+1] = chi
    c[k]   += a[k] * sumb + b[k] * suma - chi
    suma   += a[k]
    sumb   += b[k]
    sumav  = oneoverr * sumav + oneoverrm1 * a[k]
    sumbv  = oneoverr * sumbv + oneoverrm1 * b[k]
  // contribute from diagonal pairs
  alpha = ( 2 - s ) / ( s * s - s )
  for( k = 0; k < N - 2; k++ )
    ckk    = a[k] * b[k]
    c[k+2] += alpha * ckk
    c[k+1] += ( 1 - alpha ) * ckk
  return c
}
```

The resulting profile $c_i G_{2D}(v_i, r)$ shares the same set of Gaussians as the input profiles, allowing easy profile addition. The downward reflectance and transmittance profiles R_{12}^+ and T_{12}^+ for a two-layer material are computed using:

$$R_{12}^+ = R_1^+ + T_1^+ * R_2^+ * T_1^- * \sum_{i=0}^{K} (R_1^- * R_2^+)^i$$

$$T_{12}^+ = T_1^+ * T_2^+ * \sum_{i=0}^{K} (R_1^- * R_2^+)^i$$

where the number of interlayer scattering events K is not likely required to exceed 5 [d'Eon et al. 2007; Donner et al. 2008].